Materials Advances

Accepted Manuscript

This article can be cited before page numbers have been issued, to do this please use: S. U. Din, S. Waheed, A. Khan, J. Razzokov, A. Ibragimov and S. Haq, *Mater. Adv.*, 2026, DOI: 10.1039/D6MA00304D.

ROYAL SOCIETY OF CHEMISTRY

rsc.li/materials-advances

View Article Online
DOI: 10.1039/D6MA00304D

ARTICLE

Role of Metabolites in Regulating Size Distribution, Structural Stability, Morphology and Biological Performance of Green-Synthesized Silver Nanoparticles via *Celtis australis Extract*

Received 00th January 20xx,
Accepted 00th January 20xx

DOI: 10.1039/x0xx00000x

Salah Ud Din[a], Sharoz Waheed[a], Abdulhameed Khan[b], Jamoliddin Razzokov[c-e], Aziz Ibragimov[f], Sirajul Haq[c, g]*

The plant mediated synthetic approach is an environment-friendly and cost-effective process for the preparation of nanomaterials. Herein this study, silver-nanoparticles (Ag.NPs) were fabricated using *Celtis australis (C. australis)* as capping agent. Synthesis of Ag.NPs was performed using various concentrations of plant extract and precurosr salt solutions labelled as SO-1, SO-2, SO-3 and SO-4. XRD is used for structural and crystallinity analysis of synthesized Ag-NPs and among the products, the one obtained by 40:60 ratio are highly crystalline. The SEM provides information about the morphology and the DLS results shows that the SO-1 has large particle size which might due to the agglomeration of the particles as less repulsion nature is depicted by the zeta potential analysis. Narrow size distribution indicates that particles are uniform size and PdI values show that the samples are monodispersed. FTIR spectrum of Ag-NPs showed the chemical functional groups and gave details about the composition confirmation of synthesized materials. UV-visible spectroscopy of Ag-NPs was used to find the λ_{max} values and band gap energies. The antioxidant capacity of Ag-NPs was observed using a method called ABTS free radical scavenging evaluation and highest activity was found for SO-4 with IC_{50} value of 37.57 µg/mL. The antibacterial action of Ag-NPs was studied against *S. aureus* and *E. coli* by using an agar well diffusion strategy and an increase was seen in the activity with increasing concentration of the samples.

1. Introduction

Nanotechnology has experienced a recent surge in popularity because it enables the development of known bulk materials with new features and explored their multiple potentials by reducing their sizes. Nanoparticles are compact particles or suspensions that have a size extending from 10 to 1000 nm and due to this diminutive size, nanoparticles exhibit unique characteristics than the bulk analogue, including greater surface area, enhanced reactivity, and dissimilar optical and magnetic attributes (Nikam, Ratnaparkhiand, & Chaudhari, 2014) (Ealia & Saravanakumar, 2017). Recently, the metallic nanoparticles gained much attention due to their applications in healthcare sector, farming, biomedical engineering, and many others due to their proven effectiveness as antimicrobial substances (Carmona, Benito, Plaza, & Recio-Sánchez, 2017). The microbicide potential metallic nanomaterials have vastly investigated against the drug resultant strains, which are developed due to overuse of antibiotics and difficult to treat with common strategies (Zhou et al., 2025). Further, the free radical generates due to different biochemical process and highly reactive, attacked on the on bio-potent molecules and initiate a chain reaction. To cover-up all these, the multifunctional metallic nanoparticles playing a significant role to control the growth of the drug resistant microbes and capped the free radicals to avoid their hazardous effect on the living organisms.

The Ag-NPs prepared by the oxidation of silver atoms possess distinctive characteristics in terms of their physical and chemical behaviors, enable them for promising biomedical applications, i.e., wound healing and cancer treatment (Belaiche *et al.,* 2021). The antifungal, antiviral, antibacterial, and anti-cancer effects of Ag-NPs are widely investigated and are found to be a possible alternative for the handling of several infections (Iqbal *et al.,* 2019). They also possess distinctive electrical and optical characteristics that make them valuable for applications in solar cells, sensors, electronic and photonics, due to their exceptional properties (Danish *et al.,* 2022). Hundreds of research study are conducted for the preparation of Ag-NPs by using chemical and physical methods and all these methods have their own merits and demerits but one thing is common among them that they are expensive and not user/eco-friendly. In comparison to these methods, the green method for the preparation of metallic nanomaterials are more diversified as it is cost-effective and user/eco-friendly (Pradheesh, Suresh, Suresh, & Alexramani, 2020). The process where the plant portion extract involve in the synthesis of NPs is more reliable and widely followed techniques for the synthesis of nanomaterial especially Ag-NPs that do not rely on harmful chemicals. The plant extract containing phytochemicals that act as reducing and capping agents and the product obtained

[a] *Department of Chemistry, University of Azad Jammu and Kashmir, Muzaffarabad 13100, Pakistan.*
[b] *Department of Biotechnology, University of Azad Jammu and Kashmir, Muzaffarabad 13100, Pakistan.*
[c] *Institute of Fundamental and Applied Research, National Research University TIIAME, Kori Niyoziy 39, 100000 Tashkent, Uzbekistan.*
[d] *Department of Natural Sciences, Karshi State Technical University, Mustaqillik Avenue street 225, Kashkadarya 180100, Uzbekistan.*
[e] *Department of Biotechnology, Tashkent State Technical University, Universitet 2, Tashkent 100095, Uzbekistan.*
[f] *Institute of General and Inorganic Chemistry, Uzbekistan Academy of Sciences, 100170 Tashkent, Uzbekistan.*
[g] *School of Engineering, Central Asian University, Tashkent 111221, Uzbekistan.*

through this process is more stable (R. Li *et al*., 2019). By manipulating factors such as pH, temperature, and duration of the reaction, it is possible to regulate the size and morphology of the NPs (Sathiya *et al*., 2014).

The European hackberry tree, known as *C. australis*, is being utilized in this research to synthesize Ag_2O NPs, is a vital resource for hill communities as it provides high-quality green fodder for livestock when other sources are scarce. Its timber is used to making variety of items such as tool handles, cups, sporting goods, agricultural equipment paper and pulp (Singh, Bhatt, & Prasad, 2006). In sub-continent traditional medicine, *C. australis* holds significant value as a natural remedy for treating a variety of ailments related to skin conditions such as pimples, as well as musculoskeletal injuries such as bone fractures, contusions, sprains, and joint pains (Hatamian, Rezaei Nejad, Kafi, Souri, & Shahbazi, 2020). This plant is highly regarded for its therapeutic properties and has been used for centuries as a natural alternative to modern medicine (Badoni, Semwal, Badoni, Kothiyal, & Rawat, 2011). The leaves and fruits of *C. australis* plant provides soothing effect and have been utilized in conventional medicine for treating conditions such as heavy menstrual bleeding, digestive disorder, and abdominal pain (Demır, Doğan, Özcan, & Haciseferoğullari, 2002).

Despite the large number of data reported on the green synthesis of Ag-NPs, the mechanistic role of the phyto-metabolites concentration in determining the morphology, structural stability, size distribution and biological potency yet report. Further, the *C. australis* extract has not been used for the synthesis of nanomaterials and a systematic concentration controlled bio-directing role remains unclear. Thereby, this study is planned to fill the gap by elucidating the concentration dependent particles growth, morphological variation and explore structure-activity correlation to offer a tunable and sustainable pathway for engineering a n efficient Ag-NPs. In this study, we are reporting the green synthesis of Ag-NPs using leaf extract of *C. australis* for the first time as a capping and reducing agent and were characterization by FTIR, UV-visible spectroscopy, SEM, XRD, DLS, and Zeta potential techniques. Antibacterial and antioxidant activities were performed using dose-depended pathway. The main goal of the study was to see effect of the metabolites on the structural and biological properties of the Ag-NPs. For this purpose, different concentration of leaves extract used for the synthesis of Ag-NPs and significant variation is observed in the structural and optical properties.

2. Experimental Section

2.1 Reagents

The reagents used this research work are silver nitrate ($AgNO_3$), sodium hydroxide (NaOH), and distilled water (DW). The chemicals were purchased from Sigma-Aldrich used as received. Fresh and healthy leaves of *C. australis* was collected from Muzaffarabad, Azad Kashmir.

2.2 Extract formation

C. australis leaves were washed with regular tap water initially and then purified with DW to remove any dirt/debris and were dried at room's ambient temperature with absorbent paper and then chopped with a sterile chopper. A quantity of 100 g of chopped leaves was heated in 1000 mL of DW, until the appearance of dense color. Then, the resulting extract was allowed to cool down at the room's ambient temperature. The extract was filtered through Whatman filter paper, and was then spun in a centrifuge at 4000 rpm for 30 min and kept at refrigerator at 4 °C.

2.3 Fabrication of Ag-NPs (SO-1)

A stock solution 0.05 M was formed by mixing 8.49 g of $AgNO_3$ with 1000 mL of DW and a 100 mL mixture of plant extract and precursor salt (20:80) was prepared, which was stirred and subjected to heat at 75 °C. A solution of 0.1 M NaOH was used to regulate and keep the pH at 10 with continuous heating and stirring for next 2 h and the color changes were continuously monitored. Then the solution was cooled for 6 h at room temperature and the precipitate was then rinsed several times with distilled water. The precipitates were dried at 100 °C and calcined the powder at 350 °C for 4 h and stored for further use. The sample procedure was repeated by taking different concentrations of leaves extract and precursor salt solution (40:60, 60:40, and 80:20) for the preparation of SO-2, SO-3 and SO-4.

2.4 Characterization Techniques

The crystalline size, morphology, surface functional groups, stability, and size distribution of the particles in the synthesized samples were analyzed. For the identification of a crystalline material XRD (Model-JDX-3532 made in JEOL, Japan) using CuKa radiations (wavelength= 1.5418 Å) was operated. SEM used to explore surface morphology is Model JSM5910 made in JEOL, Japan having a maximum magnification of 300,000X. The 400-4000 cm^{-1} band range's unique functional groups were identified utilizing the FT-IR technique (model 8400S) using KBr pellet. The size, PdI, and zeta potential analysis of the NPs were measured using DLS. Zetasizer Nano ZSP equipment developed by Malvern panalytical technologies (based in the UK) is utilized for this purpose. The SHIMADZU 1601 spectrophotometer was utilized to measure the UV-visible spectra of NPs.

2.5 Antioxidant Activity

In this research, the potential of calcined nanoparticles of Ag-NPs to act as antioxidants was investigated. This assay determines the extent to which the radical cation $ABTS^{\bullet+}$ is converted to ABTS, which is a type of salt containing ABTS, which is indicated by a decrease in color intensity. The ABTS solution was made by combining 2.5 mM potassium persulfate and 7 mM ABTS and left to react for at least 16 h for the generation of $ABTS^{\bullet+}$ free radicals. A UV-double beam spectrophotometer was utilized to determine the absorbance (A_o) of a given solution at 734 nm. 1000 µg Ag-NPs that went under calcination were dissolved in 1000 µL of distilled water to create a solution. To perform the experiments, different amounts of the solution containing nanoparticles were mixed with 1 mL of $ABTS^{\bullet+}$ solution. The absorbance (Ai) was recorded at 734 nm. The calculation of the radical scavenging activity percentage involves measuring the difference between the absorbance of a control sample (A_o) and the absorbance of the sample being tested (A_i). During the study, ascorbic acid with the same concentrations was used as standard.

$$\%RSA = \left[\frac{A_o - A_i}{A_o}\right] \times 100 \qquad (1)$$

2.6 Antibacterial Activity

The agar well diffusion technique was employed to check the effectiveness of the Ag-samples against bacteria like *S. aureus* and *E. coli*. To grow the bacteria, nutrient agar was used. The bacterial culture that had been left to grow overnight was added to a newly prepared and sterile agar media. It was put into clean Petri plates that have been sterilized. The plates were placed in a germ-free area and left to cool and harden at the surrounding room temperature. Small wells were created in each plate using a sterilized micropipette tip and filled with suspensions of silver oxide nanoparticles. The plates were then kept at 37 ℃ overnight for incubation. The antimicrobial effectiveness of the Ag-NPs was evaluated after 24 h by observing the area where bacterial growth was prevented, which is measured in millimeters as the zone of inhibition around each well.

2.7 Phytochemical Analysis of Plant

Phytochemical analysis involves qualitative evaluation of plants. To check for different phytochemical constituents, tests were performed for flavonoids, phenol, terpenoids, cardiac glycosides, saponin, and tannins.

2.8 Test for Phenol

Phytochemicals called phenolic compounds are present in every type of plant. Plant foods are the source of phenols. They act as an antioxidant which can help to prevent heart disease, decrease inflammation, decrease the likelihood of developing diabetes, and diminish the risk of cancer (Khoddami, Wilkes, & Roberts, 2013). To find out the total phenolic contents of *C. australis*, a sample of 0.5 grams of extract from the plant was used. This extract was then treated with a substance called phenol reagent, and a color change was observed. The color change that occurred indicates that the extract contains phenolic substances.

2.8.1 Test for Flavonoid

Flavonoids are found in various plant-based sources such as fruits, vegetables, and other similar food items, which belong to a group of secondary metabolites with a polyphenolic structure. They possess diverse biological benefits, such as the ability to reduce oxidative stress, decrease inflammation, and potentially prevent or treat cancer (Panche *et al.,* 2016). A few grams of *Celtis australis* extract were mixed with a slowly added 1 percent aluminum solution, and the existence of flavonoids in the extract was revealed by the yellow color observed.

2.8.2 Test for Terpenoids (Salkowski Test)

Terpenoids are a vast and diverse group of secondary metabolites found in numerous plants. They exhibit diverse biological functions, including the ability to fight against microorganisms, combat cancer cells, and reduce inflammation in the body (Ludwiczuk *et al.,* 2017). After mixing 5 ml of ethyl acetate and 0.5 g of *C. australis* extract, 2 mL of chloroform was added to create a mixture, and then gradually adding 3 mL of concentrated H_2SO_4. This resulted in the composition of two distinct layers. The presence of terpenoids was identified by observing a reddish-brown color at the border.

2.8.3 Test for Saponin

Saponins are complex organic compounds that occur naturally in many different plants. These compounds have become increasingly popular due to their diverse range of biological effects, such as their ability to prevent ulcers, inhibit the growth of tumors, fight against microbes, and enhance the effectiveness of vaccines. Saponins are considered secondary metabolites because they are not essential to the plant's survival, but they do offer important benefits to the plant's overall health and well-being (Moghimipour & Handali *et al.,* 2015). To find out the total amount of saponins in *C. australis* extract, 20 mL of distilled ultra-pure water was added to a 2 g sample and the mixture was heated in a water bath. The mixture was filtered and then 10 ml of the filtered mixture was combined with 5 mL of distilled water. Continuous shaking of the solution resulted in the formation of froth, which served as evidence of the existence of saponins.

3. Results and Discussion

3.1 Phytochemical Analysis

The results of the phytochemical analysis of the *C. australis* plant are displayed in Table 1 shows that the aqueous extract contain flavonoids, terpenoids, phenols and saponin. All of these are hydroxyl functionalized phytochemicals, and it is assume that they will be act as a capping agent during the synthesis of Ag-NPs.

Table 1: Phytochemical screening of *C. australis*

Metabolites	Conclusion
Flavonoids	+
Terpenoids	+
Phenol	+
Cardiac glycosides	–
Tannins	–
Saponin	+

The phytochemical mediated synthesis of Ag-NPs proceeds via two step redox and capping process. The process begin with electron transfer and the hydroxyl-rich phytochemicals (Flavonoid) undergoes deprotonation in aqueous medium and become negatively charged. These deprotonated groups are highly instable and releasing electrons that reduced Ag^+ ions from $AgNO_3$ to metallic Ag^0 atoms. To reach the lower energy state, these individual atoms collides and stick together to form a tiny cluster. These nucleate cluster act as seeds and the upcoming reduced Ag^+ ions accumulate on its surface and grow into Ag-NPs via further reduction and coalescence. Without capping the Ag-NPs would keep growing into larger aggregates. Therefore, the concurrently, oxidized flavonoid (quinone form) using the lone pair of oxygen adsorb onto the nascent NPs surface via electrostatic and coordination interactions, forming a stable capping layer that prevents agglomeration and imparts colloidal stability. The overall process is summarized in Fig. 1. The phytochemicals act as a biogenic electron reservoir, where the oxidative transformation of flavonoids into quinones provides the thermodynamic driving force for Ag^+ reduction and also restrict the particle growth and ensures the colloidal integrity.

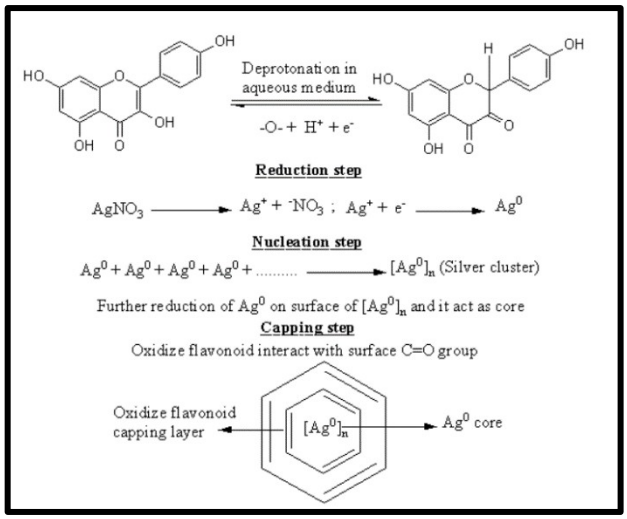

Fig. 1: Proposed reaction mechanism for the phytochemicals mediated Ag-NPs

3.2 XRD analysis

The XRD patterns as a stack plot for the Ag-NPs are shown in Fig. 2, and the diffraction peaks are located at 38º, 44º, 64º, and 77º corresponding to the hkl planes (111), (200), (220), and (311), matching with JCPDS card No. 00-004-0783 confirming the cubic structure of all the Ag-analogues with a space group of Fm3m and space number of 225. (Islam, Naqvi, Parveen, & Ahmad, 2021). The data show that the cubic unit cell has a, b and c coordinates of 4.0862 Å with 90° of all interfacial angles with a volume of 68.23 $\times 10^6$ pm^3, and density of 10.50 g.cm^{-3}. The spectra for all four samples have both sharp peaks and noisy background, indicate both crystalline and amorphous phases respectively. The crystalline phase is due to the silver and the amorphous phase may also be due to some silver portion or it might be due to the presence of phytochemicals on the surface of the samples. The d-spacing values listed in the table 2 showing a uniform increasing pattern, proposing the deposition of the phytochemicals in the interatomic spaces let the widen . The crystallite size of samples are calculated through the Debye-Scherrer (D-S) equation (eq. 2), where d (nm), k (0.94), λ (1.5406 Å) and β (FWHM) and the calculated average crystallite sizes are 28.28, 23.92, 11.01 and 12.86 nm for SO-1, SO-2, SO-3 and SO-4 respectively. Similarly, the crystallite sizes are also determined through W-H equation and the obtained plots are given as Fig. 3 and the corresponding crystallite sizes are 35.01, 14.48, 9.65 and 20.49 nm for SO-1, SO-2, SO-3 and SO-4 respectively. The data shows that the particles size following the same trend as that derived the eq. 2. The increasing trend of the crystallite sizes with the increasing extract concentration is seen, which might be due to the deposition of the metabolites on the surface of the particles (Fig. 2). These results are in close agreement with those reported in literature (Mani et al., 2021) (R. Li et al., 2019). The discrepancy in the crystallite sizes calculated by both methods are due to the fact that W-H method count the lattice strain whereas the D-S method assumes a strain free crystal.

$$D = \frac{k\lambda}{\beta cos\theta} \qquad \text{(eq. 2)}$$

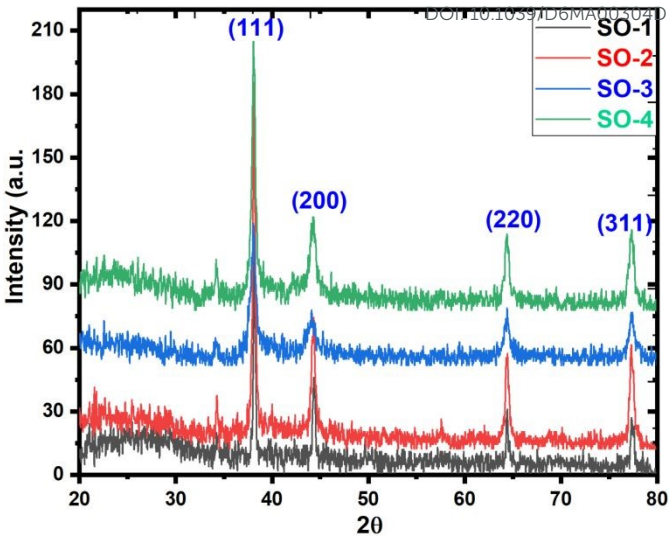

Fig. 2: XRD patterns of synthesized Ag-NPs samples

Table 2: Calculated FWHM, d-spacing and crystalline size of Ag-NPs

Sample code	Peak position	Miller indices	Theta	FWHM	d-spacing	Crystalline size
SO-1	38.43	111	19.22	0.24219	2.340293	34.74
	44.50	200	22.26	0.31076	2.033949	27.62
	64.75	220	32.38	0.3575	1.438402	26.32
	77.58	311	38.79	0.4168	1.229539	24.46
				Average (D nm)		**28.28**
SO-2	38.43	111	19.22	0.33785	2.340293	24.91
	44.50	200	22.26	0.38463	2.033949	22.32
	64.53	220	32.27	0.48785	1.442873	21.46
	77.35	311	38.36	0.37653	1.232552	27.03
				Average (D nm)		**23.92**
SO-3	38.20	111	19.11	0.82766	2.353555	10.16
	44.28	200	22.14	0.7548	2.04376	11.36
	64.53	220	32.27	0.8633	1.442873	10.88
	77.58	311	38.79	0.8766	1.229539	11.63
				Average (D nm)		**11.01**
SO-4	38.20	111	19.11	0.48134	2.353555	17.47
	44.28	200	22.14	0.83021	2.04376	10.33
	64.53	220	32.27	0.7853	1.442873	11.96
	77.35	311	38.36	0.8693	1.232552	11.71
				Average (D nm)		**12.86**

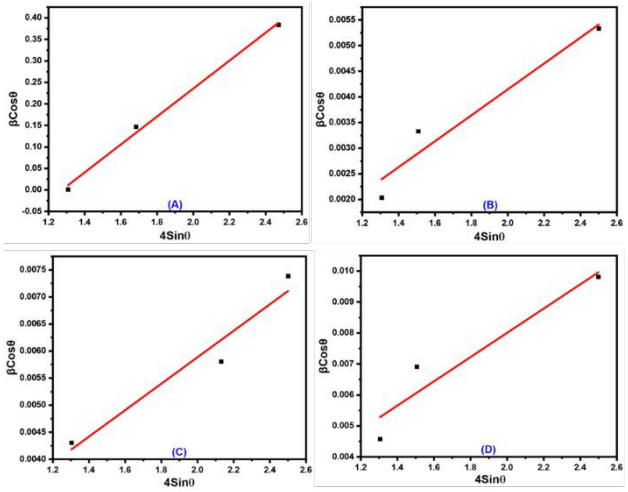

Fig. 3: W-H plots for synthesized Ag-NPs; A) SO-1, B) SO-2, C) SO-3 and D) SO-4.

View Article Online
DOI: 10.1039/D6MA00304D

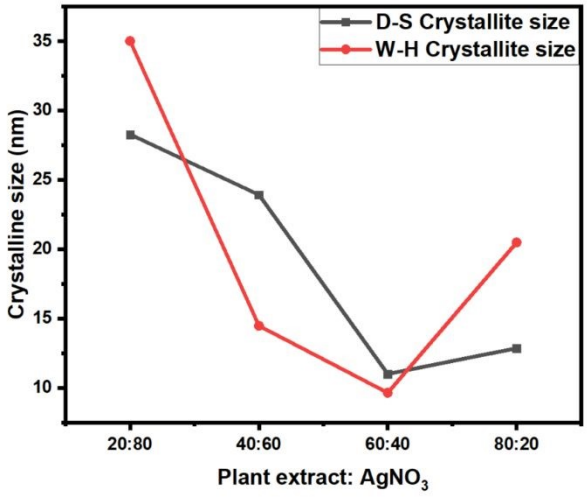

Fig. 4: Crystallite sizes variation with the reaction mixture composition

3.3 FT-IR analysis

The FTIR characterization for different samples of Ag-NPs prepared at different ratios of plant extract and precursor solution as shown in Fig. 5. For SO-1, the peak at 628 cm^{-1} shows the presence of stretching vibrations of the Ag-O bond (Laouini *et al.,* 2021) along with a sharp intensity band at 879 cm^{-1} is characteristic of the Ag-O-Ag stretching vibrations (Haq *et al*., 2018). The presence of a peak at 1245 cm^{-1} in the spectrum of NPs is linked to the C-O-C stretching vibrations of the aromatic ring (Raj, Lawrence, Silas, Jaless, & Srivastava, 2018). The presence of a peak at 1390 cm^{-1} indicates the presence of phenolic stretching vibrations (Pradheesh et al., 2020) and -CH groups (Sharma & Srivastava, 2020). The intense band at 1641 cm^{-1} indicates the presence of carbonyl (C=O) stretching vibration of flavonoids and N-H bending vibrations of the primary amides group, which usually exists in the protein (Laouini *et al.,* 2021). A broad band at 3404-3517 cm^{-1} indicates the presence of an O-H (hydroxyl) stretching vibration (R. Li *et al.,* 2019). In SO-4, an additional peak at 1034 cm^{-1} is appeared attributed to ether linkages or -C-O- (Gade *et al.,* 2010). With increasing plant extract concentration, the wavenumber increases because more secondary metabolites are present which are responsible for the shift in peaks. The carbonyls and phenolic moiety containing metabolites act as a reducing and capping agents during the synthesis of NPs (Laouini et al., 2021; Shah et al., 2019).

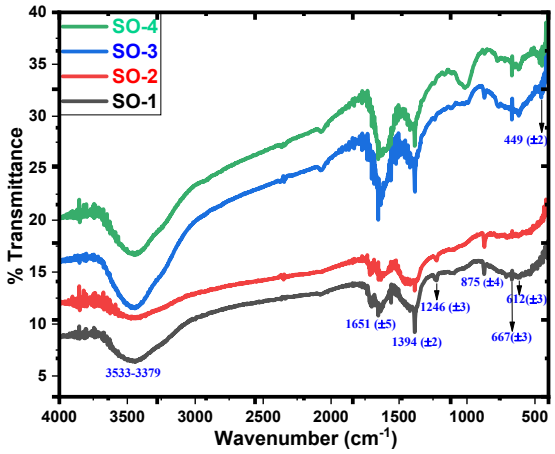

Fig. 5: FTIR spectra of the prepared Ag-NPs samples

3.4 UV-Visible analysis

Fig. 6 illustrates the UV-visible graphs of all synthesized samples, and peak for SO-1 at 466.83 nm appeared, which close to the value reported previously (Shume, Murthy, & Zereffa, 2020). The peak at 444.03 nm for SO-2 is in close agreement with value reported for the fenugreek and papaya mediated Ag-NPs (Ashokraja, Sakar, & Balakumar, 2017). The SO-3 has maxima at 412.29 nm and the obtained value is comparable to the one that was reported for the *Curcuma zanthorrhiza* aided Ag-NPs (Aiswariya & Jose, 2022). Similarly, for the SO-4 peak appeared at 375.92 nm and the value is in close proximity with that reported for Ag-NPs in literature (Rashmi *et al.,* 2020). The absorption maxima data is manipulated by using equation (3) to calculate the band gap energy (Table 3) for SO-1, SO-2, SO-3 and SO-4, which found 2.65, 2.79, 3.0, and 3.29 eV respectively (Ashokkumar, Ravi, Kathiravan, & Velmurugan, 2014). Similarly, the band gap energies was also calculated through Tauc's plot and the plots are posted as inset in Fig. 6. SThese values are in close proximity to the values reported in the literature (Fayyadh & Jaduaa Alzubaidy, 2021). The comparative trend of the SRP and the band gap energy with respect to the increasing concentration of the extract are shown in Fig. 4. The UV-visible results show a hypsochromic shift in the SPR of Ag-NPs with increasing leaves extract in the reaction (Muthukumar, Palanirajan, Shanmugam, Arivalagan, & Gummadi, 2022). This shift attributed to the maximum availability of biomolecules functionalities that act is capping agent that increase the rate of nucleation instead of growth rate. In this way, the growth rate terminates at earlier stage, the rapid particles stabilization occurred that promotes the monodispersity. The Mie theory support these findings that with decreasing particle size, the SPR shifting toward lower wavelength. The findings is supported by the XRD data, where the average crystallite size is decrease with increasing extract concentration.

$$E_{bg} = \frac{1240}{\lambda} \qquad (3)$$

View Article Online
DOI: 10.1039/D5MA00304D

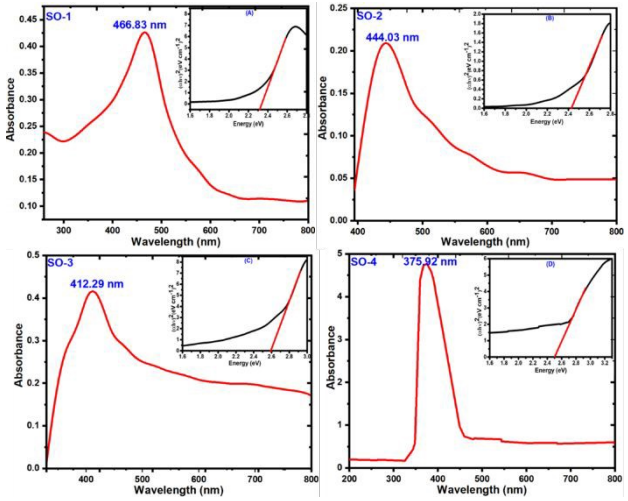

Fig. 6. UV-Visible spectra of synthesized Ag-NPs samples with Tauc's plots (A) SO-1, B) SO-2, C) SO-3 and 4) SO-4) as inset in the respective UV-Visible spectrum Ag-NPs

Table 3: λ_{max} and E_{bg} values prepared Ag-samples

Samples Code	λ_{max}	Direct spectrum band gap (E_{bg})	Tauc's Plot band gap (eV)
SO-1	466.83 nm	2.65	2.32
SO-2	444.03 nm	2.79	2.43
SO-3	412.29 nm	3.00	2.59
SO-4	375.92 nm	3.29	2.50

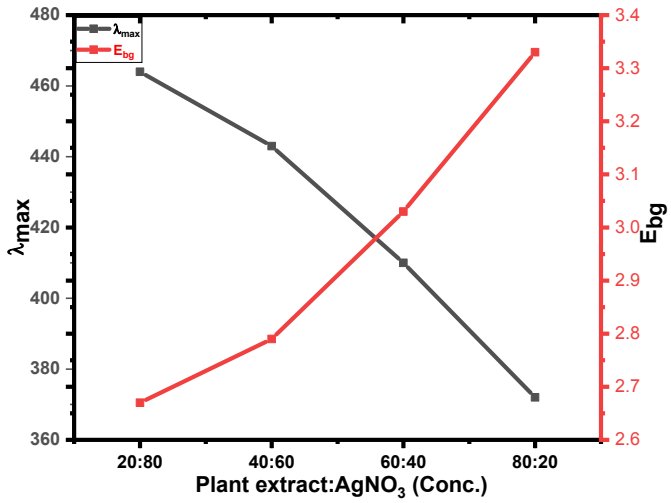

Fig. 7: representation of λ_{max} shift and band gap variation with the reaction mixture composition

3.5 DLS analysis

The DLS spectra are recorded for all the samples (Fig. 8) considering the hydrodynamic particle size and PdI and the values of particle size and PdI of Ag-NPs prepared by using different plant extract and precursor salt concentration are displayed in Table 4. A notable decrease in size of the particles is seen from SO-1 to SO-3, indication the enhanced reduction and capping by the phytochemicals led to a high nucleation rate facilitating the formation of small size particles. The afterward increase in size is usually occurred when the extract or precursor concentration reached to a point where secondary growth/particle-particle aggregation dominates over the nucleation rate (Mani et al., 2021) (Pradheesh et al., 2020) (Suresh, Pradheesh, & Ramani, 2018). The pdi values shows that SO-1 has the most uniform particles distribution as the PdI < 0.2 is considered as an ideal for the NPs, indicating the narrow size distribution and enhanced stability. Interestingly, the sample (SO-3) particles with smallest size among the samples has the highest PdI value (0.507) showing the broader size distribution reveal that despite of small average size, the sample composite of both tiny particles and larger aggregates (Sharma & Srivastava, 2020) (Muthukumar et al., 2022). The trend shows that the Z-average value decreases as the plant extract concentration increases up to 60:40. Plant extract contains various biomolecules, such as polyphenols and flavonoids, which act as reducing agents and stabilizers for nanoparticles (Rao & Paria, 2013). These biomolecules can help to control the morphology of nanoparticles by regulating the nucleation and growth processes. As the content of plant extract increases, the availability of reducing agents also increases, leading to a faster reduction rate and smaller particle sizes (Fig. 9). Plant extract concentration increases from SO-1 to SO-3, size of nanoparticles decreases but in SO-4 size again increases because there is a limit to this effect as a sometimes higher concentration of plant extract can lead to the formation of larger particles due to the aggregation of nanoparticles (Ocsoy *et al.,* 2017). The inconstancy between the crystallite size (12.86 nm) of the SO4 and hydrodynamic diameter measured by DLS was 82.85 nm is attributed to the fact that XRD exclusively measures the internal crystalline core whereas DLS determines the hydrodynamic radius, which include the hydrated layer of the plant derived capping agents and the solvent molecules adhered on the surface. Thus, the higher DLS values suggests that the NPs may exist as small, stable clusters in the aqueous phase. This phenomena is upon observed in the plant mediated synthesis, where the metabolites provides a bulky steric stabilization layer, confirming that the small crystalline subunit with size of 12.86 nm are successfully stabilized within a large organic matrix (82.85 nm).

Table 4: Z. Average (d.nm) and PdI values for Ag-NPs prepared by using different s plant extract and precursor ratio.

Samples Code	Z. Average (nm)	PdI
SO-1	103.3	0.162
SO-2	57.67	0.452
SO-3	41.72	0.507
SO-4	82.85	0.258

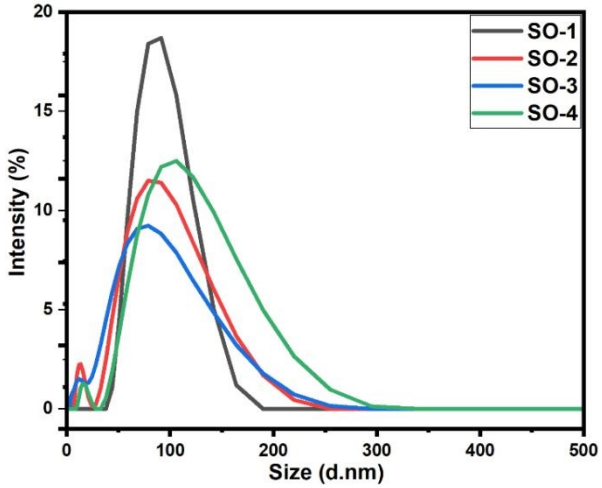

Fig. 8: DLS plots of the prepared Ag-NPs samples

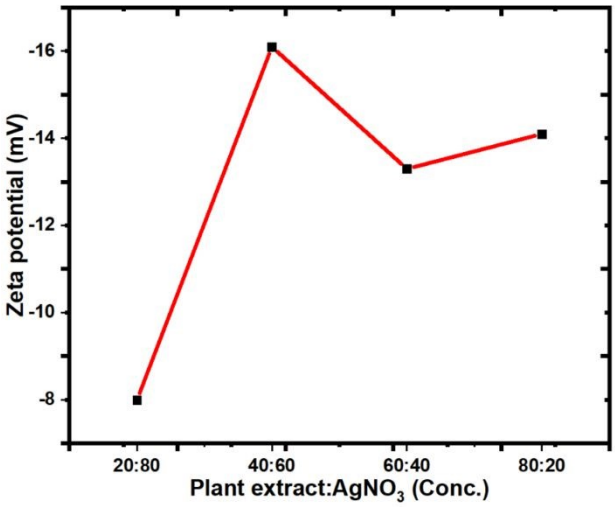

Fig. 9: Graphical representation of size distribution and PdI variation with the reaction mixture composition

3.6 Zeta potential analysis

The Zeta potential analysis of all the synthesized Ag-NPs are performed and values are listed in table 5, where the highest zeta potential value (-16.1 mV) was recorded for SO-2 suggesting the highest stability of the samples as compared to other analogues i.e. SO-1, SO-3 and SO-4 show the zeta potential values -7.99, -13.33, and -14.1 mV, respectively. A negative numerical value assigned to the synthesized NPs implies that their surface carries a negative charge, which can lead to electrostatic repulsion between the particles and prevent them from agglomerating or sticking together. This indicates that the Ag-NPs synthesized using a green method exhibit stability when suspended in a liquid medium. The negative value is due to the capping operation of various metabolites present in the leaf extract of *C. australis* and the obtained results are consistent with the *C. haematocephala* and *R. virgata* derived silver-based NPs (Raja, Ramesh, & Thivaharan, 2017) (Abbasi *et al.,* 2020). For So-1 two peaks are seen in the plot at -23.8 mV and 55.6 mV, revealing that the sample is composed of two or more distinct populations of particles with different zeta potentials. However, the value of -7.99 mV is the zeta potential value recorded for the overall population of Ag-NPs in the sample, presenting the average surface charge of the entire population of the sample. The comparative trend for zeta potential values of all samples is depicted in Fig. 10, showing the low negative zeta potential value for SO-1 as compared to SO-2, SO-3 and SO-4, whereas the SO-2 has the highest negative zeta potential value. Plant extract contains various secondary metabolites such as polyphenols and flavonoids, which act as reducing and capping agents. These metabolites influence the zeta potential values (Rao & Paria, 2013).

Table 5: Values of Z-P for Ag-NPs prepared by using different s plant extract and precursor ratio

Samples code	Zeta potential (mV)
SO-1	-7.99
SO-2	-16.1
SO-3	-13.3
SO-4	-14.1

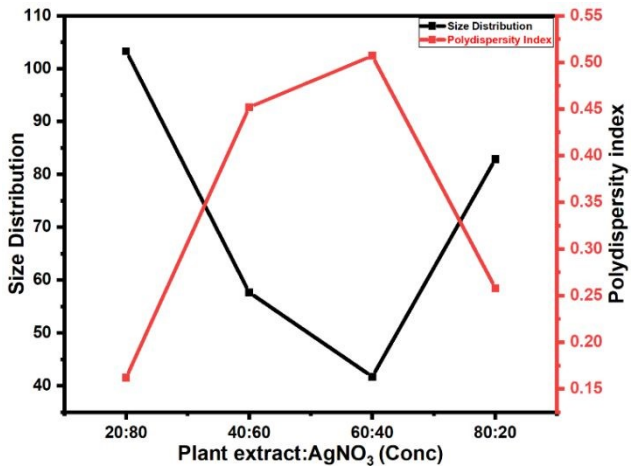

Fig. 10: Graphical representation of zeta potential variation with the reaction mixture composition

3.7 SEM analysis

The SEM analysis of the Ag-NPs samples prepared at different extract and precursor slat concentration is performed and the obtained SEM micrograph are presented in Fig. 11. The results provide visual evidence of the extract concentration of the morphology, distribution and aggregation of the sample from SO-1 to SO-4. The SO-1 image shows comparatively inform distribution which aligned with the lowest PdI value with largest hydrodynamic particles size among the prepared the samples. With increase in the plant leaves extract, the samples (SO-2 and SO-3) are going toward a transition from large particle size to small particle size, which also evident from the smallest Z-average for the SO-3. The particles of SO-2 and SO-3 samples are tend to stick together forming a non-uniform inconsistent

View Article Online
DOI: 10.1039/D6MA00304D

mixture as evident from the high PdI value (0.507). Upon further increase in the extract ratio, the SO-4 shows completely different morphology presenting a fuse matrix with cracked film surface where the larger secondary particles embedded within it. This proposed the changes in growth kinetics and suppression of the nucleation rate at a specific high concentration. The SEM analysis completely aligned with DSL data. These results show that the plant extract to precursor ratio is an important factor that determine the nucleation rate, morphology, agglomeration and stability of the resultant sample.

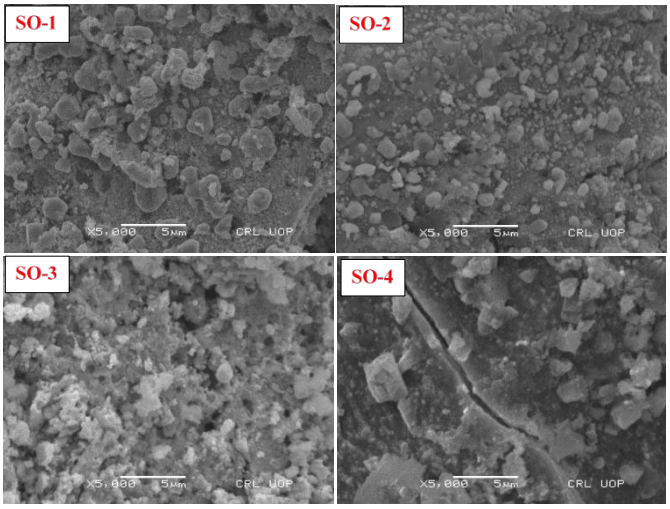

Fig. 11: SEM micrographs of synthesized Ag-NPs sample.

3.8 Antioxidant analysis

The free radicals scavenging activity of the samples was performed against the $ABTS^{\bullet+}$ and the obtained data is computed in the table 6. The activity is seen to increasing with increasing concentration of the prepared sample in the solution, confirming the dose dependent behavior of the reaction. The increase in concentration accompanied by the increase in active sites that effectively neutralizing the free radicals. Another pronounced increasing trend is seen when moved from SO-1 to SO-4, the activity efficiently increase with each passing test level. This indicates that the higher volume of the extract led to better capping of the Ag-NPs, showing that the phytochemicals present in the extract not reduce the silver ion but also remain on the surface of the Ag-NPs. In the XRD analysis in the increase in the d-spacing value also suggest the deposition of the phytochemicals in the interatomic spaces. Therefore, the utilization of the more extract in the synthesis of the Ag-NPs led to a higher density of the antioxidant functional groups on the surface of the NPs. Nearly 72 % dropped in the IC_{50} values is seen from SO-1 to SO-4 indicates that the optimization of the extract volume has significantly enhance the antioxidant potential of the Ag-NPs. The plant extract used for the synthesis of the Ag-NPs containing flavonoids, saponins, phenols, and terpenoids has synergistic effect on the particles size, stability and a richer bioactive coating resulting into higher inhibiting activity of the Ag-NP (Satpathy, Patra, Ahirwar, & Delwar Hussain, 2018).

Table 6: Percentage scavenging activity (%) of Ag-NPs prepared by using different s plant extract and precursor ratio

Sample Code	Concentration (µL)	% RSA	IC_{50} (µg/mL)
SO-1	10	18	132.65
	50	26	
	100	42	
SO-2	10	21	88.15
	50	32	
	100	56	
SO-3	10	33	49.08
	50	48	
	100	75	
SO-4	10	34	37.57
	50	56	
	100	89	

3.9 Antibacterial analysis

The antibacterial analysis of the Ag-NPs analogues reported here was performed by following well-diffusion protocols using clindamycin and ciprofloxacin as positive controls for *S. aureus* and *E. coli* respectively. The experimental photographs (Fig. 12) have clear inhibition zones that are measured in millimeter indicating the activity of the samples against respective bacteria and the data are computed in table 7. The dosage-dependent activity of the samples follows the same raising trend with increasing concentration of the sample in the wells and the highest is achieved with 20 mg/mL. During this process, the solvent shows no effect on the activity; both standard drugs have the highest activity and the activity of all the Ag-NPs analogues is less than that of the standard drug. These results are consistent with previous studies on Ag-NPs synthesized through green methods (D. Li *et al.,* 2021).

The samples are found to have stronger antibacterial activity against gram-negative bacteria compared to gram-positive bacteria. This may be due to the differences in the structure of the cell walls of these two types of bacteria. Gram-positive bacteria have a strong and rigid cell wall made of peptidoglycan, which provides resistance against mechanical rupture. In contrast, gram-negative bacteria have a thinner cell membrane and a layer of lipoprotein and lipopolysaccharide. The small size of nanoparticles facilitates their penetration into the cells of bacteria. However, the rigidity of the cell wall is due to the multiple peptidoglycan layer of gram-positive bacteria makes it less permeable compared to the thinner peptidoglycan layer of gram-negative bacteria. Therefore, Ag-NPs are more impactful

against gram-negative bacteria due to their greater permeability (Elemike, Onwudiwe, Ekennia, Sonde, & Ehiri, 2017).

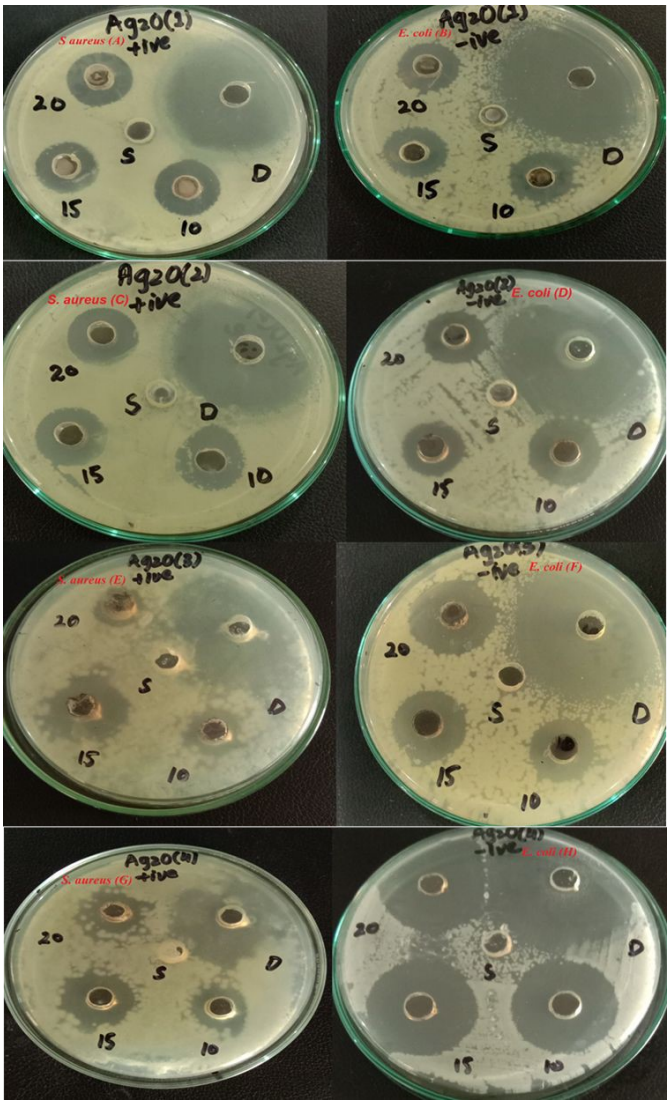

Fig. 12: Antibacterial activity of SO-1 (A, B), SO-2 (C, D), SO-3 (e, F) and SO-4 (G, H) O against *S. aureus* and *E. coli*

Table 7: Antibacterial activity of Ag-NPs against Gram-positive and Gram-negative bacteria using various concentrations

Sample Code	Microorganism	Zone of inhibition measured in millimeters				
		Positive control	10 mg/mL	15 mg/mL	20 mg/mL	Solvent
SO-1	*S. aureus*	36	18.5	18.5	19	00
	E. coli	38	19	19	19.5	00
SO-2	*S. aureus*	36	18.5	19	19.5	00
	E. coli	36	18	19	21.5	00
SO-3	*S. aureus*	35	15.5	23.5	15	00
	E. coli	38	19	21.5	25	00
SO-4	*S. aureus*	35	17.5	21.5	20.5	00
	E. coli	36	30	28	31.5	00

Regarding the potential release of Ag+ into aqueous/bacterial media, it is important to note the high stability of the synthesized Ag-NPs. The FTIR analysis (Fig. 9) clearly demonstrate the presence of robust coating of plant derived metabolites particularly the phenolic contents, which act as efficient capping agents. The literature indicates that natural biological materials provides a protective barrier that significantly retards the oxidation and subsequent dissolution of the Ag core into free ions compared to uncapped or chemically synthesized Ag-NPs. Similarly, the zeta potential data (Fig. 9 and table 5) show strong electrostatic repulsion that maintains colloidal integrity and minimizes ion leakage into the surrounding medium.

4. Conclusions

In the present study, Ag-NPs were synthesized using *C. australis* extract as a stabilizing, and reducing agent and for the preparation of Ag_2-NPs, various concentrations of plant extract and precursor solution were utilized. XRD reveals the cubic geometric shapes of the Ag-crystallites in the nano-range. The higher W-H crystallite size as compared to D-S crystallite size highlight the presence of intrinsic lattice strain induced during bioreduction process. SEM study shows a diverse morphology of the Ag-samples, and prominent changes occurred with changing the reaction conditions. The successful synthesis of Ag-NPs was confirmed through FTIR and the results show that secondary metabolites are responsible for the peak shift for the samples. The DLS results show that the size distribution of the samples ranging from 41.72 to 103.3 nm. The comparative analysis reveals a direct correlation between precursor concentration, structural dimensions and optical properties. The SO-3 has most refined architecture with smallest Z-average of 41.72 nm and the corresponding crystallite size of almost 10 nm.PdI values showed that samples (So-1 to So-3) are monodisperse and negative zeta potential results confirmed the stability of Ag-NPs. The observed expansion in band gap from 2.32 eV to 2.59 eV as the particle size decreases suggesting the presence of quantum confinement effect within the plant mediated NPs. Percentage scavenging analysis of the Ag-NPs was observed at different concentrations corresponding to IC_{50} value. Ag-NPs show good antioxidant potential. The show good activity against *E. coli* and the difference in the activity is might be due to the structural difference between different bacterial species.

Author Contributions

Sharoz Waheed – Formal analysis and First draft write-up; Salah Ud Din - Supervision, Project administration, Visualization and Resources; Abdulhameed Khan – Methodology, Physicochemical analysis and validation; Jamoliddin Razzokov, Aziz Ibragimov and Sirajul Haq – Conceptualization, Methodology Software, and review and editing

Conflicts of interest

There are no conflicts of interest associated with this manuscript.

Data availability:

The datasets generated and analyzed during this study for XRD, SEM, FTIR, DLS, Zeta potential, UV-Vis, bioactivity measurements are included in this manuscript.

References

Abbasi, B. A., Iqbal, J., Nasir, J. A., Zahra, S. A., Shahbaz, A., Uddin, S., . . . Mahmood, T. (2020). Environmentally friendly green approach for the fabrication of silver oxide nanoparticles: Characterization and diverse biomedical applications. Microscopy Research and Technique, 83(11), 1308-1320.

Aiswariya, K., & Jose, V. (2022). Bioactive molecules coated silver oxide nanoparticle synthesis from Curcuma zanthorrhiza and HR-LCMS monitored validation of its photocatalytic potency towards malachite green degradation. Journal of Cluster Science, 1-12.

Ashokkumar, S., Ravi, S., Kathiravan, V., & Velmurugan, S. (2014). RETRACTED: Synthesis, characterization and catalytic activity of silver nanoparticles using Tribulus terrestris leaf extract: Elsevier.

Ashokraja, C., Sakar, M., & Balakumar, S. (2017). A perspective on the hemolytic activity of chemical and green-synthesized silver and silver oxide nanoparticles. Materials Research Express, 4(10), 105406.

Badoni, R., Semwal, D. K., Badoni, P. P., Kothiyal, S. K., & Rawat, U. (2011). A novel bacteriohopanoid from Celtis australis L. bark. Chinese Chemical Letters, 22(1), 81-84.

Belaiche, Y., Khelef, A., Laouini, S. E., Bouafia, A., Tedjani, M. L., & Barhoum, A. (2021). Green synthesis and characterization of silver/silver oxide nanoparticles using aqueous leaves extract of Artemisia herba-alba as reducing and capping agents. Revista Romana de Materiale, 51(3), 342-352.

Carmona, E. R., Benito, N., Plaza, T., & Recio-Sánchez, G. (2017). Green synthesis of silver nanoparticles by using leaf extracts from the endemic Buddleja globosa hope. Green Chemistry Letters and Reviews, 10(4), 250-256.

Danish, M. S. S., Estrella-Pajulas, L. L., Alemaida, I. M., Grilli, M. L., Mikhaylov, A., & Senjyu, T. (2022). Green synthesis of silver oxide nanoparticles for photocatalytic environmental remediation and biomedical applications. Metals, 12(5), 769.

Demır, F., Doğan, H., Özcan, M., & Haciseferoğullari, H. (2002). Nutritional and physical properties of hackberry (Celtis australis L.). Journal of Food Engineering, 54(3), 241-247.

Ealia, S. A. M., & Saravanakumar, M. (2017). A review on the classification, characterisation, synthesis of nanoparticles and their application. Paper presented at the IOP conference series: materials science and engineering.

Elemike, E. E., Onwudiwe, D. C., Ekennia, A. C., Sonde, C. U., & Ehiri, R. C. (2017). Green synthesis of Ag/Ag2O nanoparticles using aqueous leaf extract of Eupatorium odoratum and its antimicrobial and mosquito larvicidal activities. Molecules, 22(5), 674.

Fayyadh, A. A., & Jaduaa Alzubaidy, M. H. (2021). Green-synthesis of Ag2O nanoparticles for antimicrobial assays. Journal of the Mechanical Behavior of Materials, 30(1), 228-236.

Gade, A., Gaikwad, S., Tiwari, V., Yadav, A., Ingle, A., & Rai, M. (2010). Biofabrication of silver nanoparticles by Opuntia ficus-indica: in vitro antibacterial activity and study of the mechanism involved in the synthesis. Current Nanoscience, 6(4), 370-375.

Haq, S., Rehman, W., Waseem, M., Meynen, V., Awan, S. U., Saeed, S., & Iqbal, N. (2018). Fabrication of pure and moxifloxacin functionalized silver oxide nanoparticles for photocatalytic and antimicrobial activity. Journal of Photochemistry and Photobiology B: Biology, 186, 116-124.

Hatamian, M., Rezaei Nejad, A., Kafi, M., Souri, M. K., & Shahbazi, K. (2020). Interaction of lead and cadmium on growth and leaf morphophysiological characteristics of European hackberry (Celtis australis) seedlings. Chemical and Biological Technologies in Agriculture, 7(1), 1-8.

Hulla, J., Sahu, S., & Hayes, A. (2015). Nanotechnology: History and future. Human & experimental toxicology, 34(12), 1318-1321.

Iqbal, S., Fakhar-e-Alam, M., Akbar, F., Shafiq, M., Atif, M., Amin, N., . . . Farooq, W. A. (2019). Application of silver oxide nanoparticles for the treatment of cancer. Journal of Molecular Structure, 1189, 203-209.

Islam, S. N., Naqvi, S. M. A., Parveen, S., & Ahmad, A. (2021). Application of mycogenic silver/silver oxide nanoparticles in electrochemical glucose sensing; alongside their catalytic and antimicrobial activity. 3 Biotech, 11(7), 342.

Khoddami, A., Wilkes, M. A., & Roberts, T. H. (2013). Techniques for analysis of plant phenolic compounds. Molecules, 18(2), 2328-2375.

Laouini, S. E., Bouafia, A., Soldatov, A. V., Algarni, H., Tedjani, M. L., Ali, G. A., & Barhoum, A. (2021). Green synthesized of Ag/Ag2O nanoparticles using aqueous leaves extracts of Phoenix dactylifera L. and their azo dye photodegradation. Membranes, 11(7), 468.

Li, D., Chen, S., Zhang, K., Gao, N., Zhang, M., Albasher, G., . . . Wang, C. (2021). The interaction of Ag2O nanoparticles with Escherichia coli: Inhibition–sterilization process. Scientific Reports, 11(1), 1703.

Li, R., Chen, Z., Ren, N., Wang, Y., Wang, Y., & Yu, F. (2019). Biosynthesis of silver oxide nanoparticles and their photocatalytic and antimicrobial activity evaluation for wound healing applications in nursing care. Journal of Photochemistry and Photobiology B: Biology, 199, 111593.

Ludwiczuk, A., Skalicka-Woźniak, K., & Georgiev, M. (2017). Terpenoids Pharmacognosy (pp. 233-266): Elsevier.

Mani, M., Harikrishnan, R., Purushothaman, P., Pavithra, S., Rajkumar, P., Kumaresan, S., . . . Kaviyarasu, K. (2021). Systematic green synthesis of silver oxide nanoparticles for antimicrobial activity. Environmental research, 202, 111627.

Moghimipour, E., & Handali, S. (2015). Saponin: properties, methods of evaluation and applications. Annual Research & Review in Biology, 207-220.

Muthukumar, H., Palanirajan, S. K., Shanmugam, M. K., Arivalagan, P., & Gummadi, S. N. (2022). Photocatalytic degradation of caffeine and E. coli inactivation using silver oxide nanoparticles obtained by a facile green co-reduction method. Clean Technologies and Environmental Policy, 24(4), 1087-1098.

Nikam, A. P., Ratnaparkhiand, M. P., & Chaudhari, S. P. (2014). Nanoparticles–an overview. Int. J. Res. Dev. Pharm. Life Sci, 3, 1121-1127.

Ocsoy, I., Demirbas, A., McLamore, E. S., Altinsoy, B., Ildiz, N., & Baldemir, A. (2017). Green synthesis with incorporated hydrothermal approaches for silver nanoparticles formation and enhanced antimicrobial activity against bacterial and fungal pathogens. Journal of Molecular Liquids, 238, 263-269.

Panche, A. N., Diwan, A. D., & Chandra, S. R. (2016). Flavonoids: an overview. Journal of nutritional science, 5, e47.

Pradheesh, G., Suresh, S., Suresh, J., & Alexramani, V. (2020). Antimicrobial and Anticancer Activity Studies on Green

View Article Online
DOI: 10.1039/D6MA00304D

Synthesized Silver Oxide Nanoparticles from the Medicinal Plant Cyathea nilgiriensis Holttum. International Journal of Pharmaceutical Investigation, 10(2).

Raj, A., Lawrence, K., Silas, N., Jaless, M., & Srivastava, R. (2018). Green synthesis and charcterization of silver nanoparticles from leafs extracts of rosa indica and its antibacterial activity against human pathogen bacteria. Oriental Journal of Chemistry, 34(1), 326.

Raja, S., Ramesh, V., & Thivaharan, V. (2017). Green biosynthesis of silver nanoparticles using Calliandra haematocephala leaf extract, their antibacterial activity and hydrogen peroxide sensing capability. Arabian Journal of Chemistry, 10(2), 253-261.

Rao, K. J., & Paria, S. (2013). Green synthesis of silver nanoparticles from aqueous Aegle marmelos leaf extract. Materials Research Bulletin, 48(2), 628-634.

Rashmi, B., Harlapur, S. F., Avinash, B., Ravikumar, C., Nagaswarupa, H., Kumar, M. A., . . . Santosh, M. (2020). Facile green synthesis of silver oxide nanoparticles and their electrochemical, photocatalytic and biological studies. Inorganic Chemistry Communications, 111, 107580.

Sathiya, P., Geetha, D., & Ramesh, P. (2014). Green synthesis of Silver Nanoparticles using Psidium guajava leaf extract and their Characterization. Indian Streams Research Journal, 4(8).

Satpathy, S., Patra, A., Ahirwar, B., & Delwar Hussain, M. (2018). Antioxidant and anticancer activities of green synthesized silver nanoparticles using aqueous extract of tubers of Pueraria tuberosa. Artificial cells, nanomedicine, and biotechnology, 46(sup3), 71-85.

Shah, A., Haq, S., Rehman, W., Waseem, M., Shoukat, S., & Rehman, M.-u. (2019). Photocatalytic and antibacterial activities of paeonia emodi mediated silver oxide nanoparticles. Materials Research Express, 6(4), 045045.

Sharma, S. N., & Srivastava, R. (2020). Silver oxide nanoparticles synthesized by green method from Artocarpus Hetrophyllus for antibacterial and antimicrobial applications. Materials Today: Proceedings, 28, 332-336.

Shume, W. M., Murthy, H. A., & Zereffa, E. A. (2020). A review on synthesis and characterization of Ag2O nanoparticles for photocatalytic applications. Journal of Chemistry, 2020, 1-15.

Singh, B., Bhatt, B., & Prasad, P. (2006). Variation in seed and seedling traits of Celtis australis, a multipurpose tree, in central Himalaya, India. Agroforestry Systems, 67(2), 115-122.

Suresh, S., Pradheesh, G., & Ramani, V. A. (2018). Biosynthesis and characterization of CuO, MgO and Ag2O nanoparticles, anti inflammatory activity and phytochemical screening of the ethanolic extract of the medicinal plant Pavetta indica Linn. Journal of Pharmacognosy and Phytochemistry, 7(4), 1984-1990.

Zhou, Y., Chen, Y., Zhao, W., Wang, J., Chen, Y., Wen, H., He, Y., Li, N., Mao, H., & Cui, Y. (2025). Nanoflower-mediated gallium-protoporphyrin IX complex for intracellular antibacterial and immunomodulatory effects in macrophage-targeted therapy. *ACS Nano*, *19*(26), 23659–23679.

View Article Online
DOI: 10.1039/D6MA00304D

Data Availability Statement:

The datasets generated and analyzed during this study for XRD, SEM, FTIR, DLS, Zeta potential, VU-Vis, bioactivity measurements are included in this manuscript.